Volume 6 | Number 5 | June 2019 | Pages 837–1082

Materials Horizons

rsc.li/materials-horizons

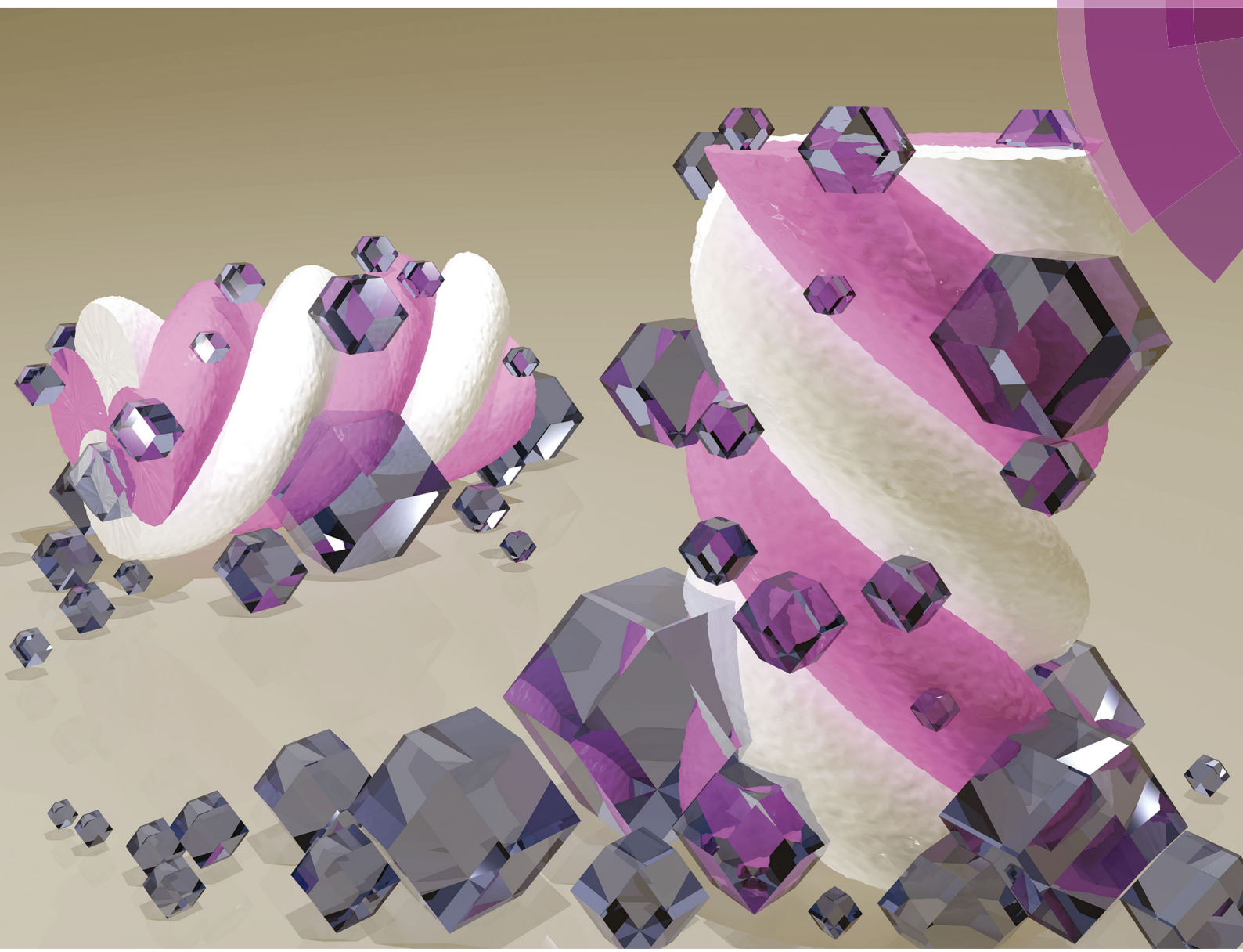

ISSN 2051-6347

ROYAL SOCIETY OF CHEMISTRY | Celebrating IYPT 2019

COMMUNICATION
Christian J. Doonan, Paolo Falcaro *et al.*
Carbohydrates@MOFs

Materials Horizons

COMMUNICATION

View Article Online
View Journal | View Issue

Cite this: *Mater. Horiz.*, 2019, 6, 969

Received 16th December 2018,
Accepted 20th February 2019

DOI: 10.1039/c8mh01611a

rsc.li/materials-horizons

Carbohydrates@MOFs†

Efwita Astria, ‡[a] Martin Thonhofer,‡[ab] Raffaele Ricco, [a] Weibin Liang,[c] Angela Chemelli,[d] Andrew Tarzia, [c] Karen Alt,[e] Christoph E. Hagemeyer, [e] Johannes Rattenberger,[f] Hartmuth Schroettner,[f] Tanja Wrodnigg,[g] Heinz Amenitsch, [d] David M. Huang, [c] Christian J. Doonan *[c] and Paolo Falcaro *[ac]

MOFs have demonstrated outstanding properties for the protection and controlled release of different bio-entities, from proteins to living cells. Carbohydrates, as pure molecules or as a component of proteins and cells, perform essential biological functions. Thus, an understanding of the role of carbohydrates in the formation of MOF-based bio-composites will facilitate their application to biotechnology and medicine. Here, we investigate the role of carbohydrate molecular weight and chemical functionalization in the formation of carbohydrate@MOF composites. We find that chemical functionalization, such as carboxylation, that leads to an enhancement of metal cation concentration at the surface of the molecule triggers the rapid self-assembly of the MOF material, zeolitic-imidazolate framework 8 (ZIF-8). Furthermore, we determine the encapsulation efficiency and measure the release properties of the carbohydrate under controlled conditions. Our findings show that MOFs can be used to prepare a new class of biocomposites for the delivery of carbohydrate-based therapeutics.

Conceptual insights

Carbohydrate-based therapeutics are relevant drugs for the treatment of cancer, diabetes, viral and bacterial infections. Therefore the efficient encapsulation and controlled release of carbohydrates has great potential in biomedicine. Here, we present a successful strategy to trigger the spontaneous crystallization of metal–organic frameworks (MOFs) on carbohydrates. The encapsulation of carbohydrates within ZIF-8 and polymorphs (zinc-imidazolate-based MOFs) can be obtained in water. The identification of conditions suitable for the successful preparation of the composite were experimentally and computationally identified. By controlling the chemical functionalization of the carbohydrate, the formation of bio-composites can be obtained in seconds. A 100% encapsulation efficiency was obtained. The controlled release of carbohydrates from the MOF biocomposite was demonstrated. This proof-of-concept study shows that a new generation of MOF bio-composites can be exploited for biomedical applications.

Introduction

Metal–organic frameworks (MOFs) are a class of crystalline porous materials that typically possess high accessible surface areas and narrow pore size distributions. In addition, the chemical functionality, on their surface or within their pores, can be precisely tuned.[1] These unique properties have led to the exploration of MOFs for application in areas such as catalysis, gas storage, separation, microelectronics, and energy production.[2–4] In recent years, MOFs have been integrated with metallic, ceramic, and biological moieties to form novel composite materials.[5–8] In the area of MOF bio-composites, it has been shown that MOFs can be used as carriers for therapeutics ranging from small drugs[9,10] to large biomacromolecules.[11,12] In the latter case, ZIF-8 has been widely investigated.[7,8] ZIF-8, and related polymorphs,[11] can rapidly form in the presence of different biomacromolecules.[7] The synthesis can be performed by adding the ZIF-8 building blocks, 2-methylimidazole (2mIM) and Zn^{2+}, to proteins in the presence of a co-precipitating agent (*e.g.* polyvinyl pyrrolidone) to assist the protein encapsulation (a.k.a. the *de novo* approach).[13,14] Alternatively, MOF formation can be triggered exclusively by

[a] *Institute of Physical and Theoretical Chemistry, Graz University of Technology, 8010 Graz, Austria. E-mail: paolo.falcaro@tugraz.at*
[b] *Laboratory for Characterisation and Processing of Polymer, Faculty of Mechanical Engineering, University of Maribor, SI-2000, Maribor, Slovenia*
[c] *Department of Chemistry, The University of Adelaide, 5005 Adelaide, South Australia, Australia. E-mail: christian.doonan@adelaide.edu.au*
[d] *Institute of Inorganic Chemistry, Graz University of Technology, 8010 Graz, Austria*
[e] *Australian Centre for Blood Diseases, Monash University, Melbourne, Australia*
[f] *Graz Centre for Electron Microscopy (ZFE), 8010 Graz, Austria*
[g] *Institute of Organic Chemistry, Graz University of Technology, 8010 Graz, Austria*

† Electronic supplementary information (ESI) available: Additional figures, movies and experimental details. Substrates used and their formulas, schematic overviews of the performed syntheses and workups, time-dependent MOF-formation experiments induced by different carbohydrates and concentrations, yield calculations, SEM image of ZIF-8 on glass and paper, FTIR spectra of the starting materials and the obtained products, schematic of the ion-permeable spherical model, kinetics studies, UV-Vis analyses, photographs of solutions using different polysaccharides, and video showing the succesfull biomimetic mineralisation of CM-dextran. See DOI: 10.1039/c8mh01611a

‡ These authors contributed equally.

pure biomacromolecules.[16] This method, termed biomimetic mineralisation, has been successfully employed to encapsulate proteins, DNA, enzymes, and antibodies and to coat viruses and cells with MOFs.[7,8,15–17] In these biocomposites the ZIF-8 shell was shown to protect biomacromolecules from environments that typically lead to their degradation, to act as a gate for molecular transport, and to release the encapsulated biomolecules under controlled conditions.[18,19] While progress has been made toward understanding the biomimetic mineralisation process for certain biomacromolecules (*e.g.* proteins), for others, *e.g.* carbohydrates (CHs), reliable preparation protocols are not yet available (*vide infra*). Nevertheless, carbohydrate-based molecules such as polysaccharides play crucial metabolic, structural, physical, and functional roles in biological systems.[20] The number of different biologically relevant polysaccharides (also called glycans) that an organism produces (the glycome) is estimated to be 10 to 10^4 times larger than the corresponding number of proteins (the proteome).[21] Because of the incremental understanding of the biological role of glycans, their importance in medicine is progressively increasing and carbohydrate-based therapies have received considerable attention in recent years.[21–23] Pure glycans can be delivered as effective therapeutics; for example dextrin-2-sulphate was found to reduce replication of HIV-1 in patients with AIDS and to induce a gradual regression of Kaposi's sarcoma lesions.[24] The fusion of glycans with other biomacromolecules (glycosylation) can substantially modify the structure and function of proteins and lipids influencing intermolecular and intramolecular interactions; for instance, the type of glycan present on IgG1 antibodies contributes to determining their function, *e.g.* pro-inflammatory or anti-inflammatory properties.[25] Glycans can be artificially attached to proteins (glycoengineering)[26] to improve their robustness; the effectiveness of this method is evidenced by the commercially available glycosylated proteins.[27] Glycans are also active key players at the interface of viral capsids[28] and cell membranes as CHs regulate adaptation, differentiation, adhesion and signaling.[22,29,30]

Motivated by our interest in the exploitation of MOFs for biotechnological applications and the widespread use of CHs in biology,[7,8] we investigated the biomimetic mineralisation of ZIF-8 by CHs. A detailed understanding of how ZIF-8 encapsulates mono- and poly-saccharides will expand the use of MOFs in biotechnology and biomedicine.

A preliminary study that describes the facile encapsulation of polysaccharides by ZIF-8 has been recently reported.[31] In this work, the synthesis was performed by adding polysaccharides (*e.g.* dextran, molecular weight not disclosed) to a solution of 2mIM; this solution mixture was then combined with a zinc acetate solution. We have been unable to reproduce these results in our laboratory, even after varying the reported protocol (*e.g.* order of reagents, temperature, and concentration).[31] Thus, we considered the preparation of carbohydrates@MOF composites an open scientific challenge and carried out a systematic study to test CHs for the preparation of bio-MOF composites. In this present study, we investigated the role of mono-, di-, oligo-, and poly-saccharides as potential biomimetic mineralisation agents for the formation of CHs@ZIF-8. Here, we show that the encapsulation of CHs within ZIF-8 and its structural polymorphs is not general. Indeed, the majority of the CHs do not lead to the formation of MOF biocomposites. More importantly, computational and experimental data show that the chemical functionality of polysaccharides is critical to the reproducible preparation of CHs@ZIF-8. Furthermore, to highlight the potential application of biomimetic mineralisation to the release of polysaccharide-based therapeutics, we used unlabelled and fluorescein isothiocyanate-labelled carboxyl-functionalized polysaccharides to study the encapsulation and release of CHs from ZIF-8 composites. In summary, we have determined a general method for preparing CHs@ZIF-8 biocomposites, which is an important first step towards exploring these materials for the release of polysaccharide-based therapeutics and for the controlled growth of MOF shells around moieties of biological interest, such as glycosylated proteins, viruses, and cells.

Results and discussions

Biomimetic mineralisation is a term that describes the triggered formation of MOF particles or films by single biomacromolecules or more complex biological entities (*e.g.* a virus or cell).[7] In general, to ascertain whether the biomimetic mineralisation process takes place, it is necessary to compare the particle growth kinetics of water-based MOF precursor solutions with and without the presence of the biomacromolecules. Biomimetic mineralisation is confirmed when a difference in the formation time for MOF particles is observed in the presence of the biomacromolecules (*e.g.* faster production rate or larger amount of particles). Typically, biomimetic mineralisation leads to the formation of a MOF coating around the biomacromolecules that engenders MOF-based bio-composites that possess novel properties.[7] We started our investigation into the preparation of CHs@ZIF-8 composites by testing a variety of basic CH units (*i.e.* monosaccharides) as potential biomimetic mineralisation agents (Scheme 1), including neutral reducing monosaccharides such as D-glucose (1), D-mannose (2), D-galactose (3), D-xylose (4); a non reducing sugar such as methyl-β-D-glucopyranoside (5) (Table S1, ESI†); reduced sugars such as D-glucitol (6) and meglumine (7); and monosaccharides bearing a nitrogen such as *N*-acetyl-D-glucosamine (8) and D-glucosamine (9).

Then, we tested water soluble oligosaccharides such as sucrose (10), a typical disaccharide, D-gluconic acid-δ-lactone (11), the oxidized form of glucose, and maltodextrin (approximately 20 α-1,4-D-glucose units). Finally, we studied structural analogues of the probed carbohydrates such as ethylene glycol (12) and *N*-methyl-aminoethanol (13).

Initially, we followed the literature synthesis procedure that reported the successful encapsulation of carbohydrates into ZIF-8 and structural polymorphs. The specific CH was added to an aqueous solution of 2-methylimidazole (2mIM, 160 mM) then zinc acetate (40 mM in water) was added at ambient temperature to the CH/2mIM solution (Fig. S1, ESI†). To ascertain the role of CHs in ZIF-8 formation, we employed varying quantities of sugars and, as an initial test, visually evaluated the opacity of

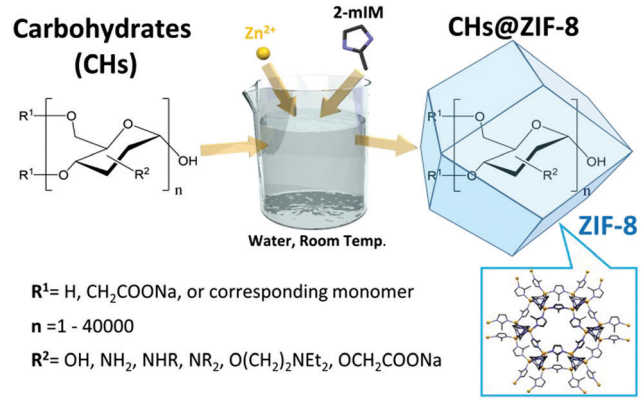

Scheme 1 Use of carbohydrates (CHs) with 2-methylimidazole (2mIM) and $Zn(OAc)_2$ to trigger the biomimetic mineralisation and the subsequent formation of carbohydrates encapsulated in ZIF-8 (CHs@ZIF-8).

the solution (Table S2 and Fig. S2, ESI†). For the majority of the sugars used, the purported biomimetic mineralisation effects were negligible (Fig. S3–S15, ESI†). Only the amino functionalized monosaccharides such as meglumine, and its analogous *N*-methyl-aminoethanol (*i.e.* 7 and 13), showed a consistent increase in turbidity with respect to the control solution (Fig. 1a).

To ascertain the formation of meglumine@ZIF-8 we fixed the concentration of the ZIF-8 precursors while increasing the concentration of the monosaccharide from 0.005 to 0.5 M. The MOF particles prepared in the presence of meglumine were collected by centrifugation, washed with water and ethanol, then dried at ambient pressure and temperature. The powder samples were investigated by X-ray diffraction (XRD) and FTIR. From the XRD analysis a diamondoid topology, **dia**, was observed for a meglumine concentration below 0.05 M; increasing the concentration of meglumine to 0.125 M or above resulted in ZIF-8 of sodalite topology, **sod**. This result suggests that the framework topology depends on the concentration of meglumine used during the synthesis (Fig. 1a(I)). After washing with water and ethanol, we performed FTIR experiments on samples prepared with different amounts of meglumine (Fig. 1a(II)). Close inspection of the data revealed vibrational bands typical of $Zn(2mIM)_2$ networks: 3120 and 2926 cm^{-1} (C–H stretching of the methyl imidazole),[32] 1420 cm^{-1} (ring stretching of methyl imidazole),[32] 900–1350 (in plane bending of imidazole ring),[33,34] 600–800 cm^{-1} (out of plane bending of imidazole ring), 421 cm^{-1} (Zn–N stretching).[33] However, we could not detect any infrared absorption band related to meglumine. Thus, despite our observation that the monosaccharide was acting as an initiator for MOF formation, the final crystalline material was found to be a single phase of Zn-imidazolate framework of **dia** or **sod** topology (Fig. 1b). It is worth highlighting that our SAXS investigation of the formation of ZIF-8 with a 0.5 M meglumine concentration did not reveal the presence of a crystalline material; however, a pattern consistent with **sod** was found after washing with ethanol. We monitored the transformation between the amorphous phase into **sod** (Fig. 1c). Despite the origin of the phase transformation remaining unclear, the importance of the washing procedure is demonstrated. For this reason, in this manuscript, the washing procedure used for the different sets of samples is specified.

The XRD and FTIR data lead us to conclude that meglumine, and the analogous *N*-methyl-aminoethanol, triggers the formation of MOF due to the presence of basic amino groups. Indeed, the addition of a base (*e.g.* triethanol amine) to MOF precursor solutions is an established method for the deprotonation of ligands and rapid crystallization of MOFs.[35,36] Controlling the local formation of base with light (*i.e.* photobase generator), MOF growth was enabled in specific locations;[37] this demonstrates that different kinetics of the MOF formation are induced by an exogenous base. To prove this hypothesis, we measured the pH of the precursor solution of the MOF in the presence of an increasing amount of meglumine. We ascertained that

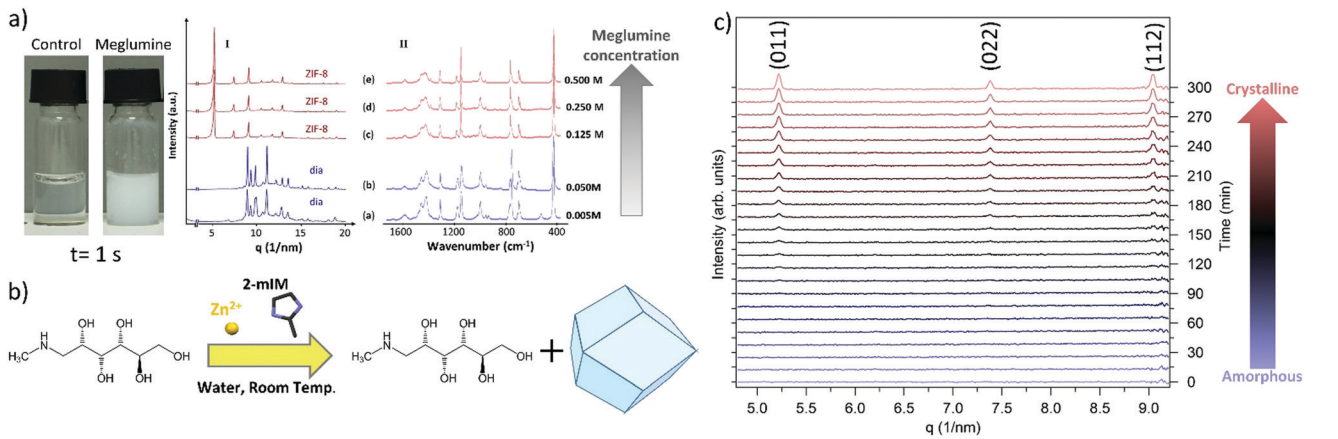

Fig. 1 (a) Photograph of a control sample (2mIM, $Zn(OAc)_2$, and water) and the same solution in the presence of meglumine, diffraction patterns, and infrared spectra of the $Zn(2mIM)_2$ produced using different concentrations of meglumine. A topology dependence on the amount of this monosaccharide was observed. (b) Schematic that illustrates meglumine as a crystallization agent. (c) SAXS kinetics that shows the phase transition from amorphous $Zn(2mIM)_2$ to sodalite triggered by the presence of ethanol. The formation of sodalite was detected by the presence of the three peaks related to the (011), (022), and (112) reflections. The (011) reflection was observed after 120 min from the injection of ethanol in the water suspension of amorphous $Zn(2mIM)_2$ particles.

the pH of the solution was in the 12–14 range (Table S3, ESI†), thus confirming the basicity of meglumine. Under specific conditions, other monosaccharides (*e.g.* D-glucose, methyl-α-D-glucopyranoside, D-glucitol, D-gluconic acid δ-lactone, D-glucosamine hydrochloride, *N*-acetyl-D-glucosamine, and D-xylose) appeared (visual inspection) to promote biomimetic mineralisation; we believe that they influence the ligand deprotonation (see details in Table S3, ESI†). To understand the effect that the preparation methods have, we studied different mixing procedures and reaction temperatures for methyl-α-D-glucopyranoside (5), glucitol (6), and meglumine (7) (Fig. S16–S18, ESI†). While meglumine induced a cloudy solution, inducing solution turbidity with the other CHs required elevated reaction temperature and/or sonication. More importantly, for the entire set of small CHs tested, FTIR analysis carried out on the solid powders after washing (H_2O and EtOH) did not provide any evidence for the encapsulation of CHs within zinc-imidazolate-based MOFs (Fig. S19–S22, ESI†).

Given these data we turned our attention to the role of the CH molecular weight in the formation of CHs@MOFs. We selected a series of dextrans of different molecular weights (*i.e.* 6, 40, and 70 kDa) as potential biomimetic mineralisation agents. Close visual inspection of these reactions gave no indication of rapid MOF formation (Table S4, ESI†). To assess these reactions more quantitatively, we performed a kinetic assessment of particle formation for 40 and 70 kDa dextran using UV-Vis spectroscopy. The solution transmittance was probed with an incident wavelength of 595 nm (Fig. S23, ESI†). No change in transmittance was observed over a time period of 30 min for either dextran. Furthermore, the change in transmittance of the negative control solution (*i.e.* a solution without the biomacromolecules) did not differ significantly from the ones containing the dextran molecules. As a positive control, bovine serum albumin (BSA) was used as the biomacromolecule; in this case, a decrease in the transmitted radiation was measured due to the formation of BSA@MOF particles. Combined, these experiments provide evidence that dextrans, regardless of molecular weight, do not induce the rapid formation of MOF-based biocomposites. To assess if the molecular structure of the polymer could play a role in the formation of a composite, we tested maltodextrin and dextran (Fig. S24, ESI†). Again, no evidence of biomimetic mineralisation was detected. Finally, we investigated solid-state CHs (cellulose) to ascertain if the surface could trigger the formation of ZIF-8. As a control, we used a glass slide. From our SEM images and FTIR investigations at 30 s and 30 min, both substrates were ineffective for inducing the growth of ZIF-8 or its polymorphs; however, within 24 hours some particles can be observed on both glass and cellulose (Fig. S25–S32, ESI†). Despite the different compositions tested and synthetic conditions used, we could not reproduce the result previously reported by Liang *et al.*[31] Thus, we considered that the challenge of preparing CH@MOFs using a general procedure was unresolved.

Recently, we explored the role of protein surface charge on the biomimetic mineralization of ZIF-8.[38] By modifying the protein surface charge *via* succinylation or amination, we

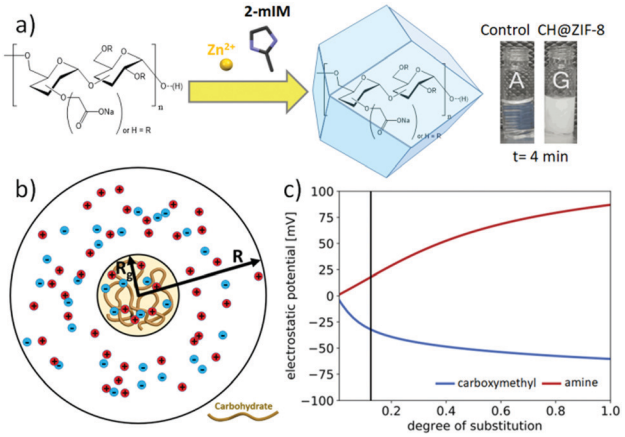

Fig. 2 (a) Schematic of the biomimetic mineralisation of CM-dextran@$Zn(2mIM)_2$ according to the infrared investigation; photograph of a control sample (2mIM, $Zn(OAc)_2$ and water) and the same solution in presence of CM-dextran. (b) Schematic of the ion-permeable sphere model of a carbohydrate molecule of radius R_g used to calculate the electrostatic potential and ion concentrations near the molecule ($R \gg R_g$ is the radius where the potential is assumed to approach zero). (c) Calculated electrostatic potential at the center of the carbohydrate *versus* degree of carboxymethyl or amino functionalization.

demonstrated that it is possible to trigger or prevent the biomimetic mineralization on several enzymes.[38] Inspired by this work, we were motivated to establish whether the chemical functionalization of CHs could produce biomimetic mineralization agents for the preparation of CHs@ZIF-8. Thus, we used commercially available amino- and carboxylate-functionalized dextrans with similar molecular weight (10 kDa and 10–20 kDa, respectively). A 1 : 4 metal-to-ligand ratio was set for consistency with prior experiments. While the amino-functionalized CH did not show evidence of biomimetic mineralisation, the solution containing the dextran with COO^- functionality (CM-dextran) showed a rapid transition from transparent to opalescent (Fig. 2a and Fig. S33 and related video ESI†). To study the influence of the CM-dextran on the pH, the concentration of the CH was varied in the 0–1.44 mg mL^{-1} range (Fig. S34, ESI†). In presence of the ligand, a *ca.* 3% maximum variation was measured, thus the role of the pH in the formation of the MOF was considered to be negligible.

The powder from the vial was collected *via* centrifugation and washed with water and ethanol (details in ESI†). The dried, powder was then analyzed by FTIR spectroscopy. Characteristic modes of carboxymethyl dextran (CM-dextran) were observed at approximately 1608 cm^{-1} that can be attributed to the COO^- stretching vibration of CM-dextran,[38,39] and at 2850–3600 cm^{-1} stretching vibrations of the OH group were observed[40] (a more comprehensive interpretation of the FTIR spectra is available in Fig. S35 ESI†). This data supports the formation of a MOF biocomposite based on CM-dextran and $Zn(2mIM)_2$.

To understand the impact of functional group substitution on the likelihood of dextran carbohydrates to seed ZIF-8 formation, we modelled the electrostatic potential and ion concentrations near charged dextrans as a function of their degree of substitution (DS) and the type of chain functionality.

Since most of the pervaded volume occupied by a dextran molecule is expected to be accessible to the ions in solution, we modelled the effect of adding positive charges (for amine functionalization, AM) or negative charges (for carboxymethyl functionalization, CM) to a neutral dextran backbone by calculating the electrostatic potential and electrolyte concentration surrounding an ion-permeable sphere (Fig. 2b) using the Poisson–Boltzmann (PB) equation (details in Fig. S36–S38, ESI†).[41] Fig. 2c shows the electrostatic potential and zinc ion concentration enhancement at the center of the ion-permeable sphere calculated as a function of DS. In this plot, the AM functionalization depletes zinc ions near dextran, while the CM functionalization enhances the Zn^{2+} concentration in and around the biomacromolecule. In particular, at the approximate DS value of the CM-dextran, the zinc ion enhancement is around 10, which was found to lead to ZIF-8 formation around various proteins.[42] Thus both the computational modelling and experimental results confirm the relevance of CH charge on the biomimetic mineralisation of $Zn(2mIM)_2$ MOFs. As an additional support to the role of the functionalization, COO^- functional groups where used to facilitate the formation of ZIF-8 on polymers and graphene.[43,44]

Having identified a CH that can be used as a reliable biomimetic mineralisation agent, we turned our attention to understanding the effect of varying the Zn^{2+}:2mIM ratio. Indeed, in a previous study,[11] we noted that the choice of Zn^{2+}:2mIM ratio affords the encapsulation of BSA within networks of different topologies, including amorphous, **sod**-, **dia**-$Zn(2mIM)_2$ and unknown phases (U12, U13, and U14).[11] Furthermore, it was experimentally demonstrated that the final topology of the composite can depend on the specific type of biomacromolecule used.[11] For the study of this CH@ZIF-8, we prepared solutions using 1:2.52 (A), 1:3.47 (B), 1:4 (C), 1:6 (D), 1:8 (E), and 1:16 (F) Zn^{2+}:2mIM ratios using a fixed concentration of CM-dextran (0.36 mg mL^{-1}). After a reaction time of 24 h, the samples were investigated by XRD (Fig. 3a).

For the sample with the lowest Zn^{2+}:2mIM ratio, the powdery material was found to be a mixture of phases dominated by U12[11] and sodalite. The biomineralised powders with 1:3.47 and 1:4 ratios were predominantly sodalite topology. A further increase of the ligand concentration (1:6) produced a pure diamond network that turned into pure sodalite for the highest ratio (1:16). The SEM images in Fig. 3b show that globular particles of *ca.* 8 μm with rough surfaces were obtained for the lowest metal/ligand ratio (1:2.52). Clusters of smaller particles were observed for 1:3.47 and 1:4 ratios (*ca.* 25 and 20 nm, respectively, Fig. S40–S41, ESI†). For the 1:6 ratio a lamellar morphology typically associated with **dia**-$Zn(2mIM)_2$ was observed, with a broad size distribution between 1 and 5 μm. This morphology was partially maintained for the 1:8 ratio,

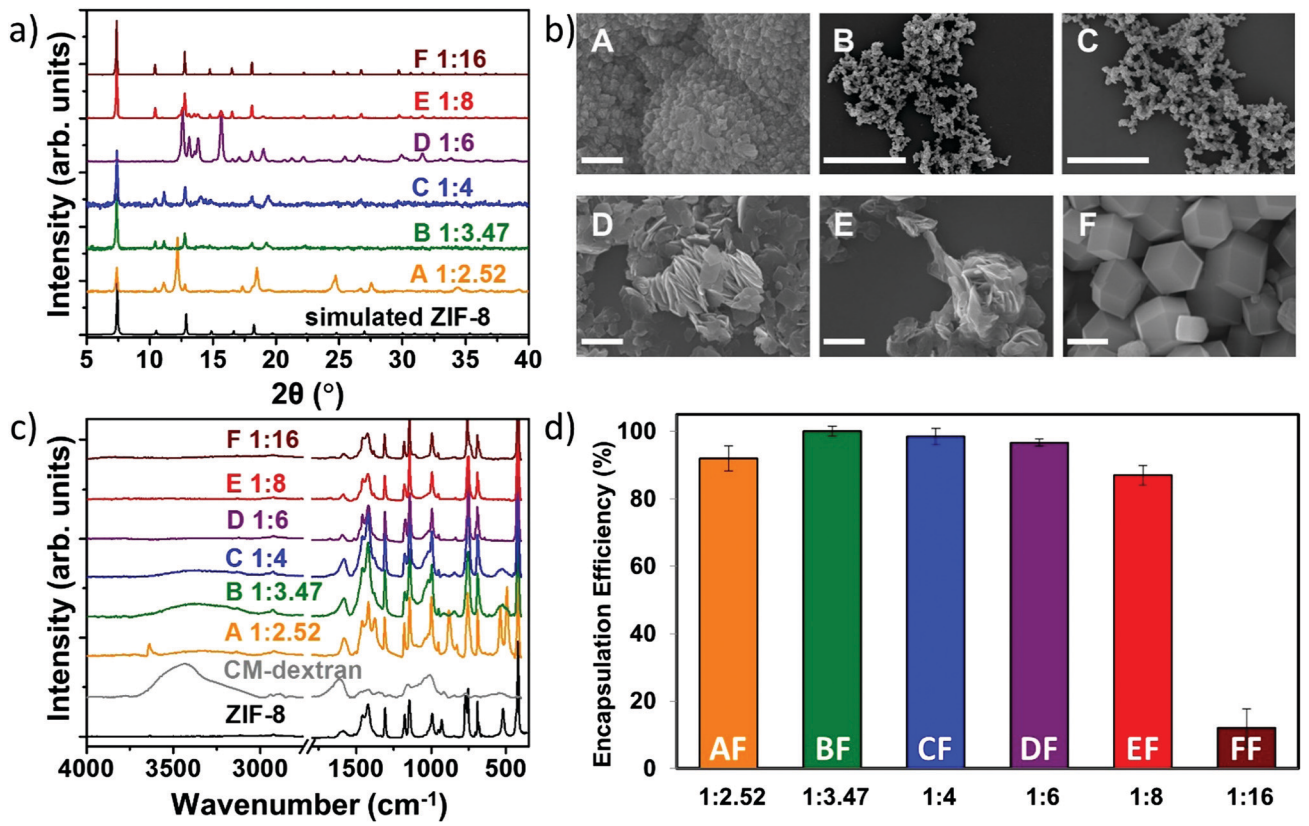

Fig. 3 (a) XRD, (b) SEM, and (c) FTIR of the CM-dextran@ZIF-8 biocomposites obtained with different metal-to-ligand ratios (A = 1:2.52, B = 1:3.47, C = 1:4, D = 1:6, E = 1:8, F = 1:16). SEM scale bar = 2 μm. (d) Encapsulation efficiency of the six systems using FITC-CM-dextran with different metal-to-ligand molar ratios (values are averages of 3 tests). The related powder X-ray diffraction plots can be found in Fig. S39, ESI.†

while for 1 : 16 typical rhombic dodecahedron particles of *ca.* 2.5 μm were noted.

After washing the powders with water and ethanol (procedure optimized for the removal of the CM-dextran adsorbed on the surface of ZIF-8 crystals, S42, ESI†), samples were investigated using FTIR spectroscopy (Fig. 3c). The vibrational mode at 421 cm^{-1}, found in all samples, is assigned to the Zn–N stretching mode and thus confirms the networks are composed of 2mIM connected *via* Zn nodes.[33] Additionally, both the COO^- mode at 1608 cm^{-1} and the large OH band in the region 3600–2850 cm^{-1} indicate that CM-dextran is encapsulated. Based on the intensity of the modes engendered by CH, the amount of encapsulated CH was found to depend on the metal-to-ligand ratio. For example, a higher loading of CM-dextran was measured in the sample prepared using Zn^{2+} : 2mIM = 1 : 3.47. In general, drug loading, also called encapsulation efficiency (EE), is an important parameter in drug delivery as it pertains to the amount of therapeutic within the carrier.[8] As CH-based therapeutics can be expensive and difficult to prepare,[45,46] we decided to run a quantitative assessment using a commercially fluorescein isothiocyanate-tagged CM-dextran, here named FITC-CM-dextran. Indeed, the use of FITC allows to use a UV-Vis spectrometer to study the release of the carbohydrate from the composite. The synthesis of the FITC-CM-dextran@ZIF-8 biocomposites was undertaken using all the previously tested Zn^{2+} : 2mIM ratios: 1 : 2.52, 1 : 3.47, 1 : 4, 1 : 6, 1 : 8, and 1 : 16 (here named samples AF, BF, CF, DF, EF, and FF, respectively). Then, we analysed the reaction supernatant using UV-Vis spectroscopy to quantitatively measure encapsulation efficiency (EE = 100%) at 1 : 3.47 (Fig. 3d). A progressive decrease in the encapsulated amount of FITC-CM-dextran with increasing concentration of 2mIM was measured. We believe that the progressive decrease in the encapsulation efficiency could be attributed to a competition between heterogeneous (biomolecule-mediated growth) and homogenous nucleation (facilitated by an increased metal-to-ligand ratio); however, further studies are needed to validate this hypothesis.

Based on parameters including a high EE and low amounts of 2mIM, we decided that the best procedure to synthesize CM-dextran@ZIF-8 (**sod**), was to employ Zn^{2+} : 2mIM = 1 : 3.47. Using this ratio of MOF precursors we further optimized the reaction conditions by varying the CH concentration. Thus we prepared new samples named B1, B2, B3, and B4 with 0.18, 0.36, 0.72, and 1.44 mg mL^{-1} of CM-dextran solutions, respectively. Photos were taken during the reaction to record visual evidence of biomimetic mineralisation. Simultaneously, a control sample (C, Fig. 4a), with Zn^{2+} : 2mIM = 1 : 3.47 prepared using the same conditions, excluding CH, was monitored to evaluate the biomimetic mineralisation effect induced by the different concentrations of CM-dextran. Fig. 4a shows photos taken after a reaction time of 2 seconds; all sample solutions (B1, B2, B3, and B4) rapidly turned opalescent confirming that the biomimetic mineralisation occurs.

Increasing the concentration of CM-dextran exceeding 3.24 mg mL^{-1} did not lead to appreciable biomimetic mineralisation; we hypothesize that this could be due to the excess of

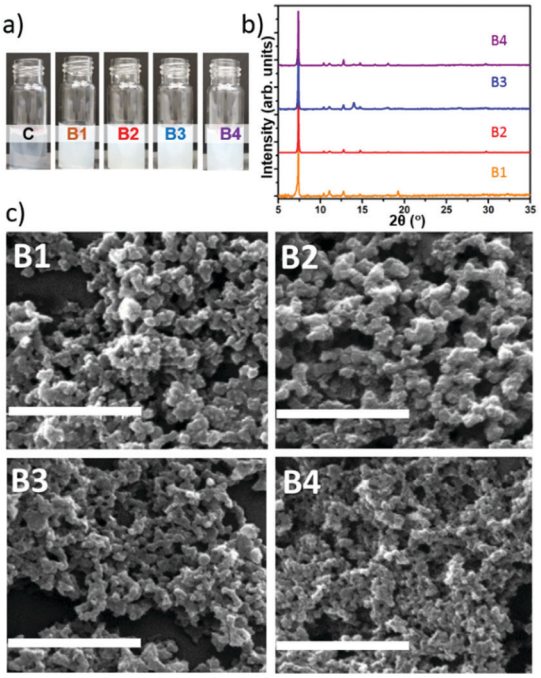

Fig. 4 (a) Photos of samples with metal/ligand ratio 1 : 3.47 and sugar concentrations of B1 = 0.18, B2 = 0.36, B3 = 0.72, and B4 = 1.44 mg mL^{-1} against control C without sugar. (b) Powder XRD of the same system. (c) SEM of samples B1, B2, B3, and B4 (scale bar: 1 μm).

COO^- removing Zn^{2+} cations from the MOF crystallization process.[47] After 24 h, the powders were centrifuged from each of the solutions and washed. We noted that different amounts of solid material were produced for each of the conditions (Table S5, ESI†). After washing, the powders were studied by FTIR (spectra reported in Fig. S43 ESI†). For all samples, vibrational modes attributed to the CH (*e.g.* OH band in the 3650–2850 cm^{-1}) and $Zn(2mIM)_2$ (*e.g.* Zn–N stretching mode at 421 cm^{-1}) were observed. This indicates that CM-dextran gave rise to CM-dextran@ZIF-8 biocomposites for each of the concentrations. To ascertain the crystallinity of the solid material, XRD analysis was conducted on samples before and after ethanol washing. For the entire set of samples (B1–4) washed only with water, sodalite was the dominant phase obtained (Fig. 4b). This demonstrates the high selectivity of this recipe for the preparation of CM-dextran@ZIF-8.

SEM images revealed the presence of particles with average particles size below 200 nm (Fig. 4c). Although we could not find specific information on the influence the size of ZIF-8 for *in vivo* drug delivery, for other particles, this size has been identified as a critical value; indeed, nanocarriers larger than 200 nm have been shown to accumulate in the liver and spleen.[48]

To study the EE as a function of the CH concentration, FITC-CM-dextran was used as a biomimetic mineralisation agent for the preparation of a set of biocomposites equivalent to the previously prepared set B. The samples prepared with FITC-CM-dextran were named set BF (*i.e.* BF1, BF2, BF3, BF4). The powders were investigated *via* SEM; surprisingly larger particles were formed (Fig. S44, ESI†). The confocal microscope (CLSM)

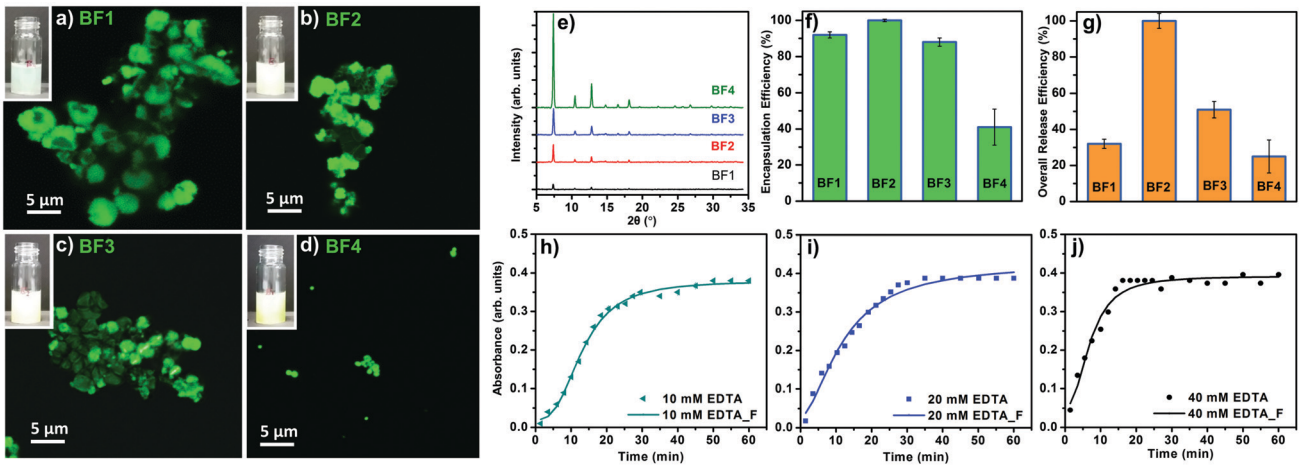

Fig. 5 (a–d) Confocal microscopy images of sample B obtained using metal-to-ligand ratio 1 : 3.47 and FITC-CM-dextran at various concentrations (BF1 = 0.18, BF2 = 0.36, BF3 = 0.72, BF4 = 1.44 mg mL^{-1}). (e) Powder XRD of the same system. (f) Encapsulation efficiency for each system (values are averages of 3 tests). (g) Overall release of the FITC-CM-dextran with respect to the original concentration used for the biomimetic mineralisation (values are averages of 3 tests). (h–j) Different release profiles on the sample BF2 using 10, 20, and 40 mM of EDTA.

confirms the different particle size (Fig. 5a–d); this variation from CM-dextran was attributed to the chemical modification of the polysaccharide.

The homogenous luminescence across the particles confirm the even distribution of the FITC-CM-dextran within the ZIF-8 particles. A PXRD analysis confirms the dominant **sod** topology for all the BF samples (Fig. 5e).

Considering the relevance of the EE in the delivery of biotherapeutics,[49] we determined the amount of FITC-CM-dextran encapsulated in ZIF-8. The assessment was performed using UV-Vis and the Lambert–Beer law with an experimental calibration of different concentrations of FITC-CM-dextran (see ESI†). As shown in Fig. 5f, the measured EE was influenced by the concentrations of the FITC-CM-dextran used as the biomimetic mineralisation agent. Intermediate concentrations of FITC-CM-dextran lead to higher EE: *ca.* 100% of the FITC-CM-dextran was encapsulated in case of BF2. For the lowest and the higher concentrations of biomacromolecules, the EE dropped to *ca.* 40% (sample BF4). We then turned our efforts to CH release. Due to the density of COO^- in the CH and the affinity for Zn^{2+} cations, we decided to investigate the amount of model drug available as a therapeutic that could be re-dissolved into its original molecular form. The dissolution process was performed leaving the biocomposites in presence of EDTA for 1 h (ESI†) at room temperature. In all cases, after etching the particles, a visual inspection revealed transparent solutions without a detectable amount of precipitate. Using UV-Vis, we calculated the percentage of FITC-CM-dextran from the correspondent CH@ZIF-8 (Fig. 5g). Again, BF2 showed the best performance as 100% of the loaded CH was available in solution after the release. For all the other samples, a percentage of the FITC-CM-dextran ranging from 25 to 51% was not available as a molecule in solution because of the combined losses during the encapsulation and release processes. We hypothesize that, during the dissolution of CH@ZIF-8, because of the strong affinity of carboxy-methyl functional groups with cations,[50] FITC-CM-dextran could coordinate Zn^{2+} to form insoluble products. Because of the ideal release performance of BF2, this sample was tested to investigate the controlled release profiles, which is another important property for drug release systems.[51] We used 3 different concentrations of EDTA (*i.e.* 10, 20 and 40 mM), and measured the release profile.

In Fig. 5h–j, the experimental data were fitted with a logistic fitting function that can be used in systems in which the dissolution of the carrier is involved.[52] In particular, this model is appropriate for ZIF-8 as it is used for hydrophobic carriers.[53–55] For the 10 mM EDTA solution, roughly 15 min were required to release 50% of the model drug; the remaining *ca.* 50% was released within 40 min. Using the 20 mM EDTA solution, in 10 min *ca.* 50% of the FITC-CM-dextran was released, while *ca.* 100% release was measured in 30 min. A further increase of the EDTA concentration (40 mM) afforded the release of 50% of the model CH in *ca.* 7 min; in 16 min a *ca.* 100% was released. These values prove that the release profile depends on the EDTA concentration, thus we demonstrated that a controlled release of CH encapsulated into ZIF-8 is possible. To ascertain the release properties using a different medium, a 100 mM sodium citrate solution (pH = 6) was tested and the release of FITC-CM-dextran from the MOF biocomposite was successfully measured (S45, ESI†).

In conclusion, we have shown that a large number of CHs do not work as biomimetic mineralisation agents. However, CHs decorated with COO^- functional groups can be employed reproducibly for the encapsulation of carbohydrates in MOFs (CH@MOFs). From our simulations this is can be attributed to a coulombic attraction between the functional groups and Zn^{2+} cations. By assessing synthesis conditions using different Zn^{2+} : 2mIM ratios and concentrations of carboxymethyl-dextran (CM-dextran) as the biomimetic mineralisation agent, we optimized a system that can form CH@ZIF-8 directly in water. We used a fluorescein isothiocyanate (FITC) tagged CM-dextran (FITC-CM-dextran) and determined conditions for the 100% encapsulation and 100% release of the model carbohydrate therapeutic.

Lastly, by varying the amount of EDTA, different release profiles were measured, showing a direct dependence between the concentration of the chelating agent and the release rate. As CHs play a number of relevant biological roles, we believe that this discovery will pave the way for the preparation of a new class of MOF-biocomposites for the delivery of carbohydrate-based biotherapeutics and for the choice of the specific CHs involved in glyco-engineering processes.

Author contributions

E. A., M. T., R. R., K. A., W. L., T. W. prepared and characterized samples, A. C. and H. A. characterized the material, H. S. and J. R. characterized part of the samples with SEM. A. T. and D. H. modeled the system, C. H. supervised part of the experiments, C. D. and P. F. conceived the idea, supervised experiments, and drafted the manuscript.

Conflicts of interest

The authors confirm that there are no conflicts to declare.

Acknowledgements

This work was supported by the Australian Research Council under the Discovery Projects Scheme (DP170103531). E. A. acknowledges the Austrian Agency for International Cooperation in Education and Research (OeAD-GmbH) for the PhD scholarship. A. T. acknowledges the Australian Government for a Research Training Program Scholarship and CSIRO Materials Science and Engineering for a PhD top-up scholarship. Chaitanya Tabib is acknowledged for the support in the laboratory. K. A. and C. H. acknowledge NHMRC (APP1098867, APP1078118). P. F. acknowledges TU Graz for the Lead Project (LP-03). R. R. acknowledges the European Union's Horizon 2020 research and innovation programme under the Marie Skłodowska-Curie grant agreement #748649 (project "MNEMONIC"). The research leading to these results has received funding from the European Research Council under the European Union's Horizon 2020 Programme (FP/2014-2020)/ERC Grant Agreement no. 771834 – POPCRYSTAL. The authors acknowledge support from the European Union's Horizon 2020 FETOPEN-1-2016-2017 research and innovation program under grant agreement 801464.

Notes and references

1 H. Furukawa, K. E. Cordova, M. O'Keeffe and O. M. Yaghi, *Science*, 2013, **341**, 1230444.
2 J. A. Mason, M. Veenstra and J. R. Long, *Chem. Sci.*, 2014, **5**, 32–51.
3 J. Gascon, A. Corma, F. Kapteijn and F. X. Llabrés i Xamena, *ACS Catal.*, 2014, **4**, 361–378.
4 J.-R. Li, R. J. Kuppler and H.-C. Zhou, *Chem. Soc. Rev.*, 2009, **38**, 1477.
5 Q.-L. Zhu and Q. Xu, *Chem. Soc. Rev.*, 2014, **43**, 5468–5512.
6 P. Falcaro, R. Ricco, A. Yazdi, I. Imaz, S. Furukawa, D. Maspoch, R. Ameloot, J. D. Evans and C. J. Doonan, *Coord. Chem. Rev.*, 2016, **307, Part 2**, 237–254.
7 C. Doonan, R. Riccò, K. Liang, D. Bradshaw and P. Falcaro, *Acc. Chem. Res.*, 2017, **50**, 1423–1432.
8 R. Riccò, W. Liang, S. Li, J. J. Gassensmith, F. Caruso, C. Doonan and P. Falcaro, *ACS Nano*, 2018, **12**, 13–23.
9 P. Horcajada, R. Gref, T. Baati, P. K. Allan, G. Maurin, P. Couvreur, G. Férey, R. E. Morris and C. Serre, *Chem. Rev.*, 2012, **112**, 1232–1268.
10 M. Lismont, L. Dreesen and S. Wuttke, *Adv. Funct. Mater.*, 2017, **27**, 1606314.
11 W. Liang, R. Ricco, N. K. Maddigan, R. P. Dickinson, H. Xu, Q. Li, C. J. Sumby, S. G. Bell, P. Falcaro and C. J. Doonan, *Chem. Mater.*, 2018, **30**, 1069–1077.
12 S. K. Alsaiari, S. Patil, M. Alyami, K. O. Alamoudi, F. A. Aleisa, J. S. Merzaban, M. Li and N. M. Khashab, *J. Am. Chem. Soc.*, 2018, **140**, 143–146.
13 F. Lyu, Y. Zhang, R. N. Zare, J. Ge and Z. Liu, *Nano Lett.*, 2014, **14**, 5761–5765.
14 F.-K. Shieh, S.-C. Wang, C.-I. Yen, C.-C. Wu, S. Dutta, L.-Y. Chou, J. V. Morabito, P. Hu, M.-H. Hsu, K. C.-W. Wu and C.-K. Tsung, *J. Am. Chem. Soc.*, 2015, **137**, 4276–4279.
15 S. Li, M. Dharmarwardana, R. P. Welch, Y. Ren, C. M. Thompson, R. A. Smaldone and J. J. Gassensmith, *Angew. Chem., Int. Ed.*, 2016, **55**, 10691–10696.
16 C. Wang, S. Tadepalli, J. Luan, K.-K. Liu, J. J. Morrissey, E. D. Kharasch, R. R. Naik and S. Singamaneni, *Adv. Mater.*, 2017, **29**, 1604433.
17 C. Wang, H. Sun, J. Luan, Q. Jiang, S. Tadepalli, J. J. Morrissey, E. D. Kharasch and S. Singamaneni, *Chem. Mater.*, 2018, **30**, 1291–1300.
18 K. Liang, J. J. Richardson, J. Cui, F. Caruso, C. J. Doonan and P. Falcaro, *Adv. Mater.*, 2016, **28**, 7910–7914.
19 K. Liang, R. Ricco, C. M. Doherty, M. J. Styles, S. Bell, N. Kirby, S. Mudie, D. Haylock, A. J. Hill, C. J. Doonan and P. Falcaro, *Nat. Commun.*, 2015, **6**, 7240.
20 A. Varki, *Glycobiology*, 2017, **27**, 3–49.
21 H. H. Freeze, *Nat. Rev. Genet.*, 2006, **7**, 537–551.
22 H. M. I. Osborn, P. G. Evans, N. Gemmell and S. D. Osborne, *J. Pharm. Pharmacol.*, 2004, **56**, 691–702.
23 S. Mitragotri, P. A. Burke and R. Langer, *Nat. Rev. Drug Discovery*, 2014, **13**, 655–672.
24 R. Duncan, *Nat. Rev. Drug Discovery*, 2003, **2**, 347–360.
25 E. Maverakis, K. Kim, M. Shimoda, M. E. Gershwin, F. Patel, R. Wilken, S. Raychaudhuri, L. R. Ruhaak and C. B. Lebrilla, *J. Autoimmun.*, 2015, **57**, 1–13.
26 R. J. Solá and K. Griebenow, *J. Pharm. Sci.*, 2009, **98**, 1223–1245.
27 L. Zhang, S. Luo and B. Zhang, *mAbs*, 2016, **8**, 205–215.
28 A. Chandrasekaran, A. Srinivasan, R. Raman, K. Viswanathan, S. Raguram, T. M. Tumpey, V. Sasisekharan and R. Sasisekharan, *Nat. Biotechnol.*, 2008, **26**, 107–113.
29 K. W. Moremen, A. Ramiah, M. Stuart, J. Steel, L. Meng, F. Forouhar, H. A. Moniz, G. Gahlay, Z. Gao, D. Chapla, S. Wang, J.-Y. Yang, P. K. Prabhakar, R. Johnson, M. dela

Rosa, C. Geisler, A. V. Nairn, J. Seetharaman, S.-C. Wu, L. Tong, H. J. Gilbert, J. LaBaer and D. L. Jarvis, *Nat. Chem. Biol.*, 2017, **14**, 156–162.
30 A. O. Tzianabos, *Clin. Microbiol. Rev.*, 2000, **13**, 523–533.
31 K. Liang, R. Wang, M. Boutter, C. M. Doherty, X. Mulet and J. J. Richardson, *Chem. Commun.*, 2017, **53**, 1249–1252.
32 Y. Hu, H. Kazemian, S. Rohani, Y. Huang and Y. Song, *Chem. Commun.*, 2011, **47**, 12694.
33 Z.-X. Low, J. Yao, Q. Liu, M. He, Z. Wang, A. K. Suresh, J. Bellare and H. Wang, *Cryst. Growth Des.*, 2014, **14**, 6589–6598.
34 M. Jian, B. Liu, R. Liu, J. Qu, H. Wang and X. Zhang, *RSC Adv.*, 2015, **5**, 48433–48441.
35 L. Huang, *Microporous Mesoporous Mater.*, 2003, **58**, 105–114.
36 M. J. C. Ordoñez, K. J. Balkus, J. P. Ferraris and I. H. Musselman, *J. Membr. Sci.*, 2010, **361**, 28–37.
37 B. K. Keitz, C. J. Yu, J. R. Long and R. Ameloot, *Angew. Chem., Int. Ed.*, 2014, **53**, 5561–5565.
38 A. Repko, D. Nižňanský, I. Matulková, M. Kalbáč and J. Vejpravová, *J. Nanopart. Res.*, 2013, **15**, 1767.
39 Y.-X. Sun, X.-Z. Zhang, H. Cheng, S.-X. Cheng and R.-X. Zhuo, *J. Biomed. Mater. Res., Part A*, 2008, **84A**, 1102–1110.
40 A. N. J. Heyn, *Biopolymers*, 1974, **13**, 475–506.
41 F. T. Wall and J. Berkowitz, *J. Chem. Phys.*, 1957, **26**, 114–122.
42 N. K. Maddigan, A. Tarzia, D. M. Huang, C. J. Sumby, S. G. Bell, P. Falcaro and C. J. Doonan, *Chem. Sci.*, 2018, **9**, 4217–4223.
43 H. Ren, L. Zhang, J. An, T. Wang, L. Li, X. Si, L. He, X. Wu, C. Wang and Z. Su, *Chem. Commun.*, 2014, **50**, 1000–1002.
44 T. Tsoufis, C. Tampaxis, I. Spanopoulos, T. Steriotis, F. Katsaros, G. Charalambopoulou and P. N. Trikalitis, *Microporous Mesoporous Mater.*, 2018, **262**, 68–76.
45 *Carbohydrate-based drug discovery*, ed. C.-H. Wong, Wiley-VCH, Weinheim, New York, 2003.
46 A. Dove, *Nat. Biotechnol.*, 2001, **19**, 913–917.
47 D. Huang, W. Wang and A. Wang, *Adsorpt. Sci. Technol.*, 2013, **31**, 611–623.
48 E. Blanco, H. Shen and M. Ferrari, *Nat. Biotechnol.*, 2015, **33**, 941–951.
49 S. D. Putney and P. A. Burke, *Nat. Biotechnol.*, 1998, **16**, 153–157.
50 R. A. A. Muzzarelli, F. Tanfani, M. Emanuelli and S. Mariotti, *Carbohydr. Res.*, 1982, **107**, 199–214.
51 S. J. Wallace, J. Li, R. L. Nation and B. J. Boyd, *Drug Delivery Transl. Res.*, 2012, **2**, 284–292.
52 F. O. Costa, J. J. S. Sousa, A. A. C. C. Pais and S. J. Formosinho, *J. Controlled Release*, 2003, **89**, 199–212.
53 K. Ghosal, A. Nanda and A. Chandra, *Pharmazie*, 2012, **67**, 147–155.
54 K. Zhang, R. P. Lively, C. Zhang, R. R. Chance, W. J. Koros, D. S. Sholl and S. Nair, *J. Phys. Chem. Lett.*, 2013, **4**, 3618–3622.
55 A. U. Ortiz, A. P. Freitas, A. Boutin, A. H. Fuchs and F.-X. Coudert, *Phys. Chem. Chem. Phys.*, 2014, **16**, 9940–9949.